(351) No 1

EG

MSC-IN-EG-65-27

PROJECT APOLLO

ANALOG SIMULATION OF A LOW FREQUENCY SPS GIMBAL SERVO IN THE APOLLO BLOCK II G&N ΔV MODE

Prepared by: Emery E. Smith, Jr.

Emery E. Smith, Jr.

Approved by: David W. Gilbert

David W. Gilbert
Chief, Engineering Simulation Branch

Approved by: R. G. Chilton

Robert G. Chilton
Deputy Chief
Guidance and Control Division

NATIONAL AERONAUTICS AND SPACE ADMINISTRATION

MANNED SPACECRAFT CENTER

June 21, 1965

SUMMARY

An analog simulation of the Apollo Block II G&N ΔV mode conducted by the Guidance and Control Division is described within. The mathematical model utilized consisted of the nonlinear, single-plane (yaw axis), rigid body equations of motion; the equations of motion of the two spring mass systems representing fuel and oxidizer slosh dynamics; and the equations of body bending dynamics for the case of the LEM in a docked position. The SCS configuration and parameters are those defined in reference 1. The cross-product steering law is utilized for the G&N ΔV mode. The data obtained from this study indicate that the SCS can be stabilized with a low frequency SPS gimbal servo; however, the operational feasibility of such a system requires that further study of the body bending dynamics be conducted.

INTRODUCTION

Because of the deletion of LTA-6 from the planned LEM test program, no vehicle will be available for modal testing until the first manned, LEM docked, orbital flight. This has caused some concern as to crew safety because the present calculated bending data could be in error enough to cause control system instability. One proposed solution to the problem is to reduce control system gain making the system less sensitive to the higher bending modes, knowledge of which is more uncertain than knowledge of the first bending mode.

The study described herein investigated the feasibility of a low frequency SPS gimbal servo. The objectives of the study were to:

a. Examine the response of the NAA SCS using a low frequency SPS gimbal servo

b. Examine the effects of body bending (first and second modes) and propellant slosh on the low frequency system

c. Examine the system as used in the G&N ΔV mode.

SYMBOL DEFINITION

A_1 - Bending coefficient, lbs

A_2 - Bending coefficient, lbs

a_x, a_y - Component of linear acceleration along the x- and y-axes, respectively, ft/sec^2

a_{x_o}, a_{y_o} - Component of linear acceleration along the x_o- and y_o-axes, respectively, ft/sec^2

B_1 - Bending coefficient, lb-sec^2

B_2 - Bending coefficient, lb-sec^2

C - Desired velocity, ft/sec

C_1 - Bending coefficient, lb

C_2 - Bending coefficient, lb

D_e - Distance from engine gimbal to engine C.M. along the engine center line, ft

D_x - Distance from engine gimbal to system C.M. along the body x-axis, ft

D_y - Distance from the system C.M. to the vehicle center line along the body y-axis, ft

d_1 - Displacement of m_1 relative to the rigid vehicle along the y-axis, ft

d_2 - Displacement of m_2 relative to the rigid vehicle along the y-axis, ft

F - Engine thrust, lbs

h_1 - Depth of fuel in tank, ft

h_2 - Depth of oxidizer in tank, ft

I_L - Clutch current, MA

I_M - Saturation value of current limiter, MA

I_{ZZ} - Moment of inertia of system about C.M., lb-ft-sec^2

SYMBOL DEFINITION - Continued

J_N - Nozzle moment of inertia about engine C.M., ft-lb-sec^2

K_1, K_2 - Spring constants in spring mass systems used to represent service module fuel slosh and oxidizer slosh, respectively, lb/ft

K_5 - Steering loop gain, deg/sec/rad

K_C - Forward gain of gimbal command, deg/deg

$K_{\dot{\delta}}$ - Gimbal rate feedback gain, deg/rad/sec

K_δ - Gimbal feedback gain, deg/rad

$K_{\dot{\psi}}$ - Attitude rate feedback gain, deg/rad/sec

K_ψ - Attitude feedback gain, deg/rad

K_ϵ - Servo amplifier gain, ma/deg

l_{x_1} - Distance from engine gimbal to sloshing mass, M_1 or M_2, ft

M_T - Total mass of the combined CSM/LEM, slugs

M_e - Engine mass, slugs

M_1 - Generalized mass for first bending mode, slugs

M_2 - Generalized mass for second bending mode, slugs

m_1 - Portion of service module fuel considered to be sloshing, slugs

m_2 - Portion of service module oxidizer mass considered to be sloshing, slugs

m_{1T} - Total fuel mass in tank, slugs

m_{2T} - Total oxidizer mass in tank, slugs

q_1 - Generalized displacement of first bending mode, ft

q_2 - Generalized displacement of second bending mode, ft

r_1 - Radius of fuel tank, ft

r_2 - Radius of oxidizer tank, ft

SYMBOL DEFINITION - Continued

S - LaPlace Operator

T - Clutch torque, ft-lb

V_{x_o}, V_{y_o} - Components of vehicle inertial velocity vector along the x_o-, y_o-axes, respectively, ft/sec

W_1, W_2 - Undamped natural frequency of spring mass systems used to represent service module fuel and oxidizer sloshing, respectively, rad/sec

X, Y - Body axis system

X_o, Y_o - Inertial axis system

ϵ - Gimbal angle error

ζ_1, ζ_2 - Damping factor in vehicle first and second bending modes, respectively, units

ζ_p - Damping factor for both fuel and oxidizer slosh, units

ξ - Root of Bessel function of first kind, order one, N.D.

τ_1 - First clutch time constant

τ_2 - Second clutch time constant

τ_3 - Third clutch time constant

τ_ϵ - Thrust misalinement (1/8" offset), (ft-lb)

$\lambda_1(Xgyro)$, $\lambda_2(Xgyro)$ - Mode shape slope of the vehicle first and second bending modes, respectively, at the rate gyro package location along the X-axis, rad/ft

$\lambda_1(Xe)$, $\lambda_2(Xe)$ - Mode shape slope of the vehicle first and second bending modes, respectively, at the SM engine gimbal location along the X-axis, rad/ft

$\lambda_1(X_{IMU})$, $\lambda_2(X_{IMU})$ - Mode shape slope of the vehicle first and second bending modes, respectively, at the inertial measuring unit platform location, rad/ft

δ - Gimbal angle, deg

δ_A - Gimbal angle feedback, deg

δ_C - Gimbal angle command, deg

δ_F - Gimbal angle due to bending, rad

SYMBOL DEFINITION - Continued

δ_{F_1} - Gimbal angle due to first bending mode, rad

δ_{F_2} - Gimbal angle due to second bending mode, rad

δ_R - Gimbal angle rate feedback, deg

ψ - Attitude, rad

ψ_C - Attitude command, deg

ψ_e - Attitude error, deg

ψ_F - Attitude feedback, deg

ψ_R - Attitude rate feedback, deg

ψ_T - Attitude plus bending effects, rad

$\phi_1(Xe)$ - Normalized displacement of first bending mode at engine hinge point

$\phi_2(Xe)$ - Normalized displacement of second bending mode at engine hinge point

DESCRIPTION OF SIMULATION

Characteristics of Simulated Vehicle

The vehicle considered was the Apollo Block II CSM with the LEM in a docked position (figure 1). A factitious worst case is studied in that for the case considered the bending parameters are determined for CSM and LEM propellant tanks full while the slosh parameters are determined for CSM tanks one quarter full and LEM tanks full. This was done to secure worst case bending and worst case sloshing simultaneously. The zero reference for the gimbal position is defined at four degrees from the vehicle center line as measured about the vehicle yaw axis to comply with the gimbal actuator geometry. A thrust misalinement, γ_ϵ, is also considered. The physical characteristics of the vehicle are listed in table I.

Equations of Motion

The single-plane (yaw axis) equations of motion included the effects of engine inertia reaction (tail-wags-dog), fuel and oxidizer sloshing, and first and second mode body bending on the vehicle dynamics. The formulae used to compute the bending and sloshing parameters are presented in table II. The complete system of equations is shown in figure 2 in block diagram form.

Control System

The autopilot used in the loop was the M-H Block K system. Included were the actuator clutch dynamics, rate gyro dynamics, a second order roll-off filter for high frequencies, and a lead-lag bending filter. The attitude was controlled by the steering loop. The commanded attitude rate was computed by taking the cross-product of the inertial acceleration and velocity to be gained $(\bar{a} \times (\bar{c} - \bar{v}))$. The yaw-axis gimbal travel was limited to ± 8.5 degrees and the rate of travel limited to ± 17.19 degrees/second.

TEST PROCEDURE

All test runs were made by placing an initial condition on the gimbal position such that the autopilot must aline the thrust vector through the center of mass during the operating cycle. When operating in the G&N ΔV mode, an initial condition was placed on the cross-axis velocity and a commanded velocity was established for the run.

RESULTS

The first series of data runs were made without the bending and slosh parameters included or the steering loop closed. Data were taken with the SPS gimbal servo natural frequency at 2.7, 2.0, 1.5, and 1.0 cps. These frequencies were attained by lowering the servo amplifier gain, K_{ϵ}, and setting the tachometer (gimbal angle rate) gain $K_{\dot{\beta}}$ at a value such that the damping in the servo loop was optimum, as determined from a linear analysis. The overall SCS gain was held constant. The results indicate that the system was stable under all of these conditions with the attitude rate gain $K_{\dot{\varphi}}$ set at about 0.5 rad/rad/sec.

The second series of data runs were made with the bending (first and second modes) and slosh parameters added to the system. Again, the response of the system was checked at 2.7, 2.0, 1.5, and 1.0 cps. The test data indicated that addition of first and second mode bending and propellant slosh to the 2.7 cps bandwidth system did not cause the system to diverge. However, the transient did show oscillations (figure 3) caused by the first bending mode.

At a bandwidth of 2 cps, the slosh and second bending mode had no appreciable effect on the system response but the first mode bending began to influence the transient response. The system oscillated near the first mode frequency and exhibited a long response time. To improve the response, the SPS damping was increased and the attitude rate gain varied. The best system characteristics were obtained with critical gimbal servo damping and the attitude rate gain about 0.5 rad/rad/sec. The system response is shown in figure 4.

The system was unstable at a bandwidth of 1.5 cps for the rate gains calculated, with the first mode bending the dominant factor causing divergence. The system was stabilized by raising the damping factor of the gimbal servo to 1.25 times critical and holding the attitude rate gain to about 0.5 rad/rad/sec. This, however, did not eliminate the oscillations caused by bending as indicated in figure 5.

Chaotic results were obtained by adding bending and slosh to the 1.0 cps system as the first bending mode caused instability in both the gimbal servo and attitude system. As was true in the previous test cases, the bending oscillations were never eliminated. The system was stabilized by raising the damping of the SPS servo to 2.0 times critical and the attitude rate gain, $K_{\dot{\varphi}}$, to about 1.0 rad/rad/sec. The time response was improved by further raising the SPS damping. A typical response of the 1.0 cps system is seen in figure 6. This response was taken with the SPS gimbal servo damping 2.5 times critical and the attitude rate gain 1.4 rad/rad/sec with zero initial conditions on the system. Because δ_o is zero, the thrust vector is misalined from the line through the center of mass by about 3.2 degrees which, in effect, gives the system a step forcing function.

No attempt was made to find the optimum SPS gimbal servo damping and attitude rate gain, $K_{\dot{\psi}}$, for the low frequency SCS, but an attempt was made to filter the bending. It was found that a second-order, low-frequency, lead-lag network would filter the bending when placed in the SPS forward loop. However, this caused diverging oscillation in the rigid body system which could not be gain stabilized.

The last series of data runs called for the addition of the steering loop to put the system in the G&N ΔV mode. A desired velocity of $C = 4000$ ft/sec in the X_0 direction was set and the cross-product steering gain K_5 was varied to check the control capabilities. K_5 was found to have a wide range of values where control was good and the autopilot was not appreciably affected.

Concluding Remarks

The simulation of the system detailed in figures 1 and 2 shows that the SCS containing a low-frequency SPS gimbal servo can be made stable, but that further study of the first mode bending effect would be necessary to qualify the servo for operational use.

Further SCS studies are planned and will be specified in forthcoming presimulation reports. These studies will investigate:

1. Bending parameter variation to determine the tolerance of the SCS to errors in the calculated parameters.

2. Effects of gimbal actuator compliance on SPS and SCS stability (reference 2).

3. Digital autopilot sampling and quantization effects on CSM control system stability (reference 3).

REFERENCES

1. "Thrust Vector Control System Analytic Model," NAA XTASI-24, April 22, 1964

2. "Proposed Analog Simulation Study of the Effects of SPS Compliance on the Apollo Block I SCS in a Thrust Vector Control Mode," E. E. Smith, February 23, 1965.

3. "Analog Simulation of Digital Autopilot Thrust Vector Control of the CSM," E. H. Simon, March 4, 1965.

TABLE I

CONSTANTS

Quantity		Value	
A_1		30660	lbs
A_2		-16400	lbs
B_1		58.26	$lb\text{-}sec^2$
B_2		-33.8	$lbpsec^2$
C		4000	ft/sec
C_1		2140	lb
C_2		-1145	lb
D_e		.667	ft
D_x		21.52	ft
D_y		.3067	ft
F		21900	lb
h_1		6.95	ft
h_2		6.95	ft
I_M		600	ma
I_{ZZ}		363,838	$lb\text{-}ft\text{-}sec^2$
J_N		220	$lb\text{-}ft\text{-}sec^2$
K_1		156.1	lb/ft
K_2		310	lb/ft
K_c		3.78	deg/deg
K_δ		57.3	deg/rad
K_ψ		57.3	deg/rad
K_ϵ	SPS natural frequency,	2.7 cps	321 ma/deg
	" " "	2.0 "	174 "
	" " "	1.5 "	98 "
	" " "	1.0 "	43.4 "

TABLE I - Continued

Quantity	Value	
l_{x_1}	4.65	ft
M_e	220	slugs
M_T	1975	slugs
M_1	2810	slugs
M_2	2810	slugs
m_1	14.1	slugs
m_2	32.3	slugs
m_{1T}	117	slugs
m_{2T}	233	slugs
r_1	1.87	ft
r_2	2.12	ft
ω_1	11.5721	rad/sec
ω_2	58.4791	rad/sec
ω_{p1}	3.32	rad/sec
ω_{p2}	3.1	rad/sec
ζ_1	.015	N.D.
ζ_2	.020	N.D.
ζ_p	.005	N.D.
f	1.841	N.D.
τ_1	1/30	sec
τ_2	1/50	sec
τ_3	1/60	sec
τ_e	228	ft-lb

TABLE I - Continued

Quantity	Value	
λ_1(XGYRO)	-.1745	rad/ft
λ_2(XGYRO)	.08375	rad/ft
$\lambda_1(X_e)$	-.1800	rad/ft
$\lambda_2(X_e)$	.1082	rad/ft
$\lambda_1(X_{IMU})$	-.1745	rad/ft
$\lambda_2(X_{IMU})$	.08725	rad/ft
$\phi_1(X_e)$	1.4	ft/ft
$\phi_2(X_e)$	-0.75	ft/ft

TABLE II

BENDING EQUATIONS

$$A_i = F\,\phi_i\,(X_e)$$

$$B_i = M_e D_e\,\phi_i\,(X_e) - J_N\,\lambda_i\,(X_e)$$

$$C_i = F\,\phi_i\,(X_e)\,\left(\frac{4}{57.3}\right)$$

PROPELLANT SLOSH EQUATIONS

$$m_i = \frac{2\,m_{iT} \cdot \tanh\,(\not{\varepsilon}\,h_i/r_i)}{\not{\varepsilon}(h_i/r_i)\,(\not{\varepsilon}^2 - 1)}$$

$$K_i = \frac{2\,m_{iT} \cdot \tanh\,(\not{\varepsilon}\,h_i/r_i)}{h_i\,(\not{\varepsilon}^2 - 1)} \cdot \frac{F}{M_T}$$

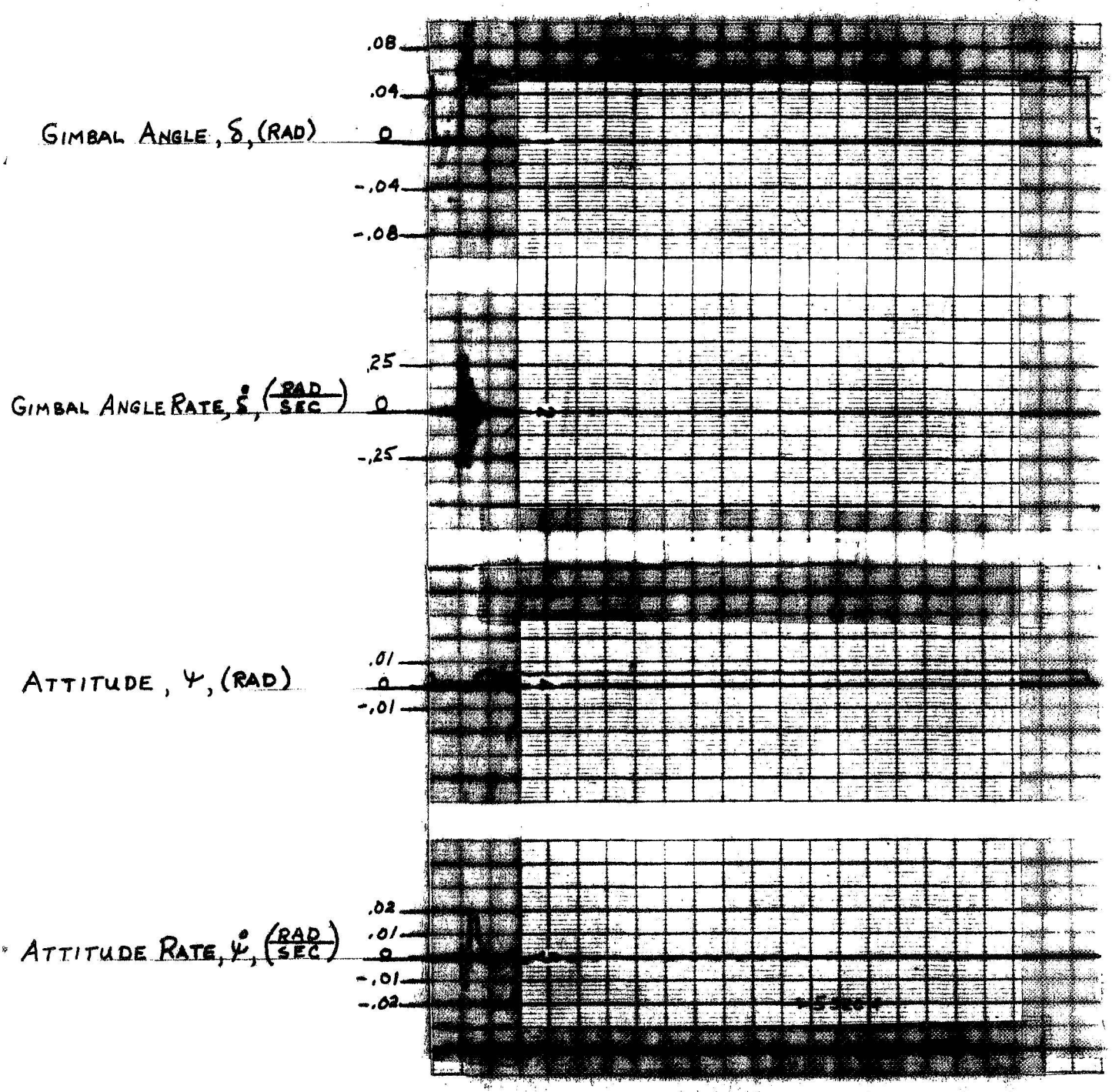

RESPONSE OF 2.7 CPS SYSTEM

FIGURE 3

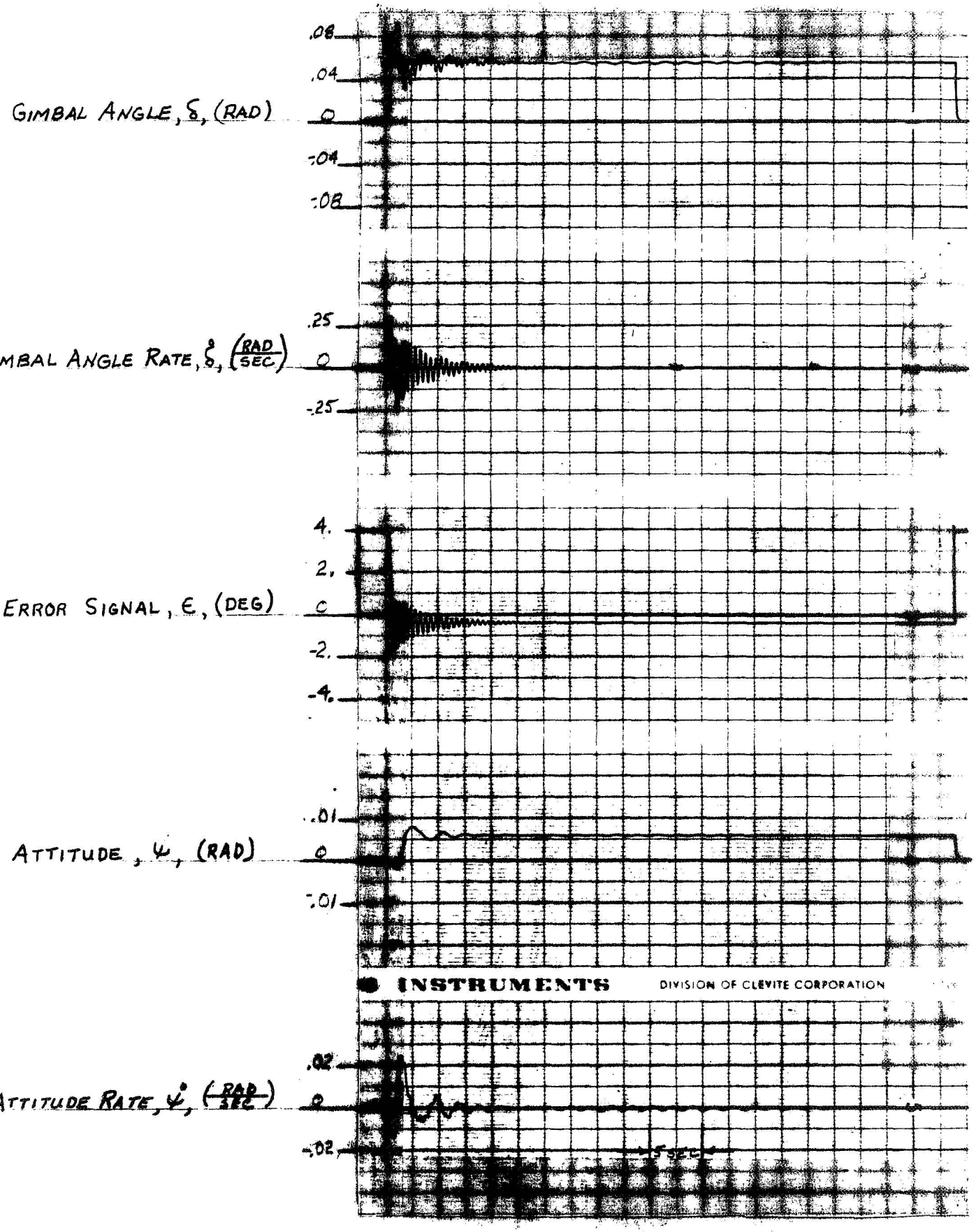

RESPONSE OF 2.0 CPS SYSTEM
FIGURE 4

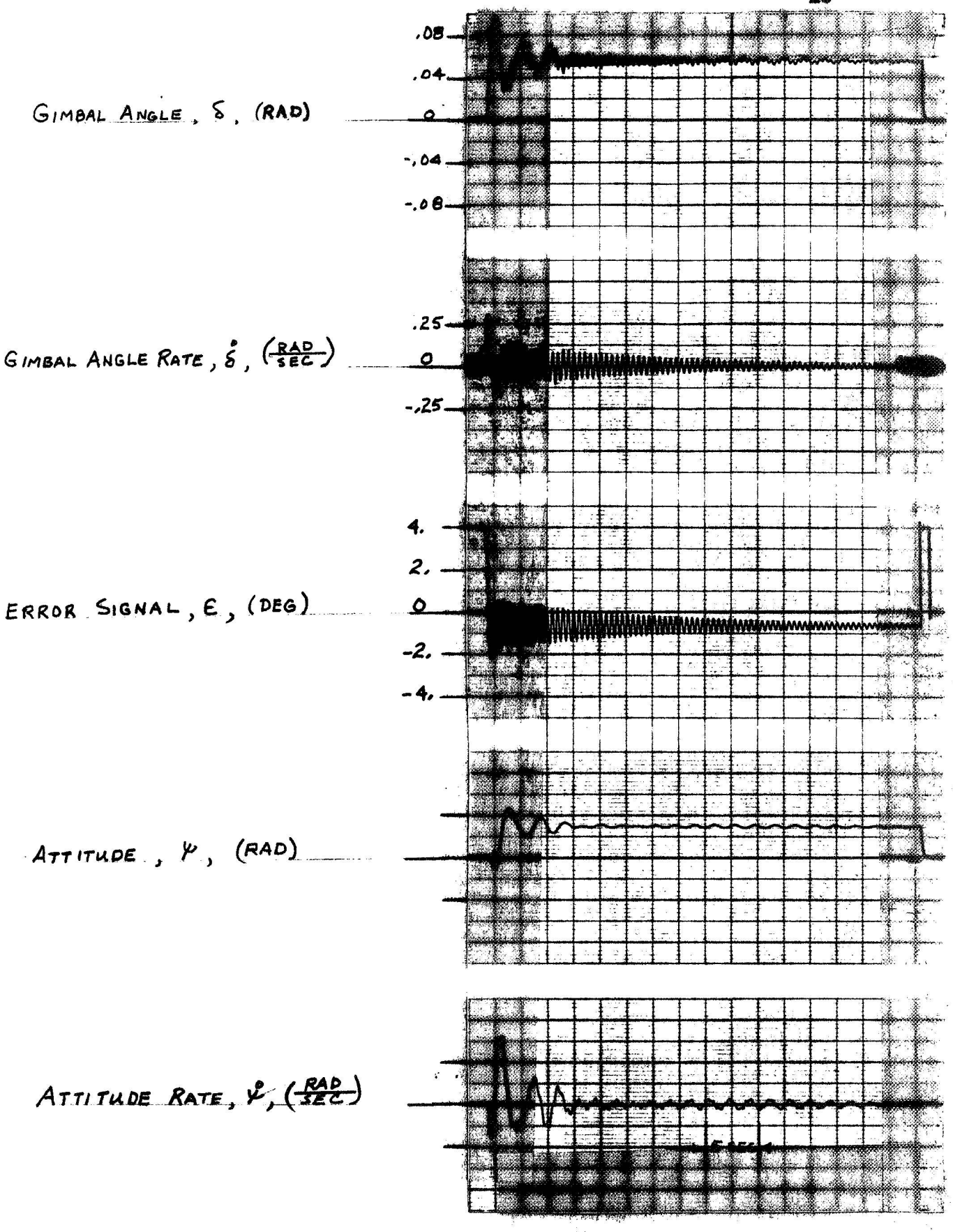

RESPONSE OF 15CPS SYSTEM
FIGURE 5

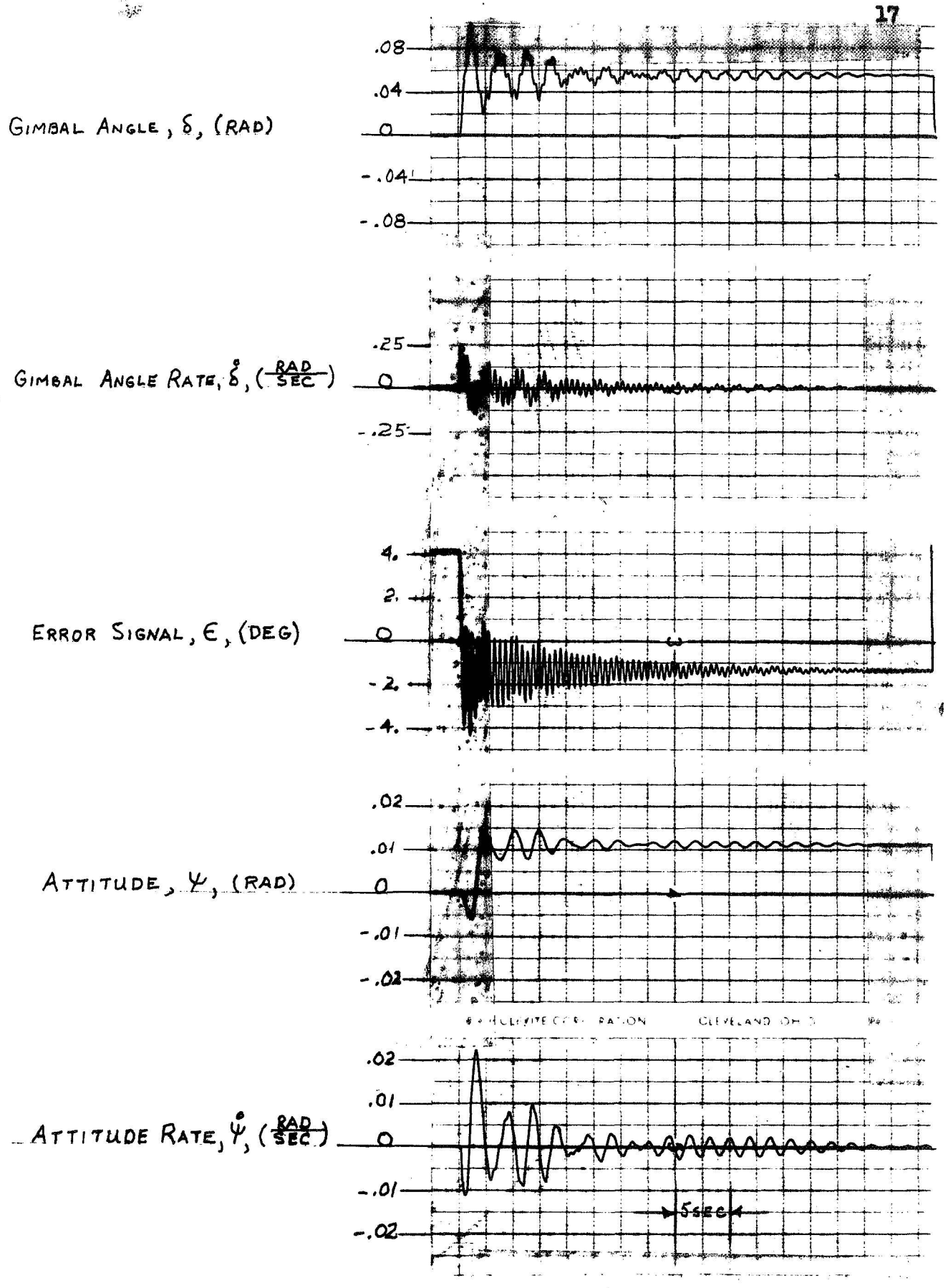

RESPONSE OF 1 CPS SYSTEM

FIGURE 6

CSM - LEM DOCKED

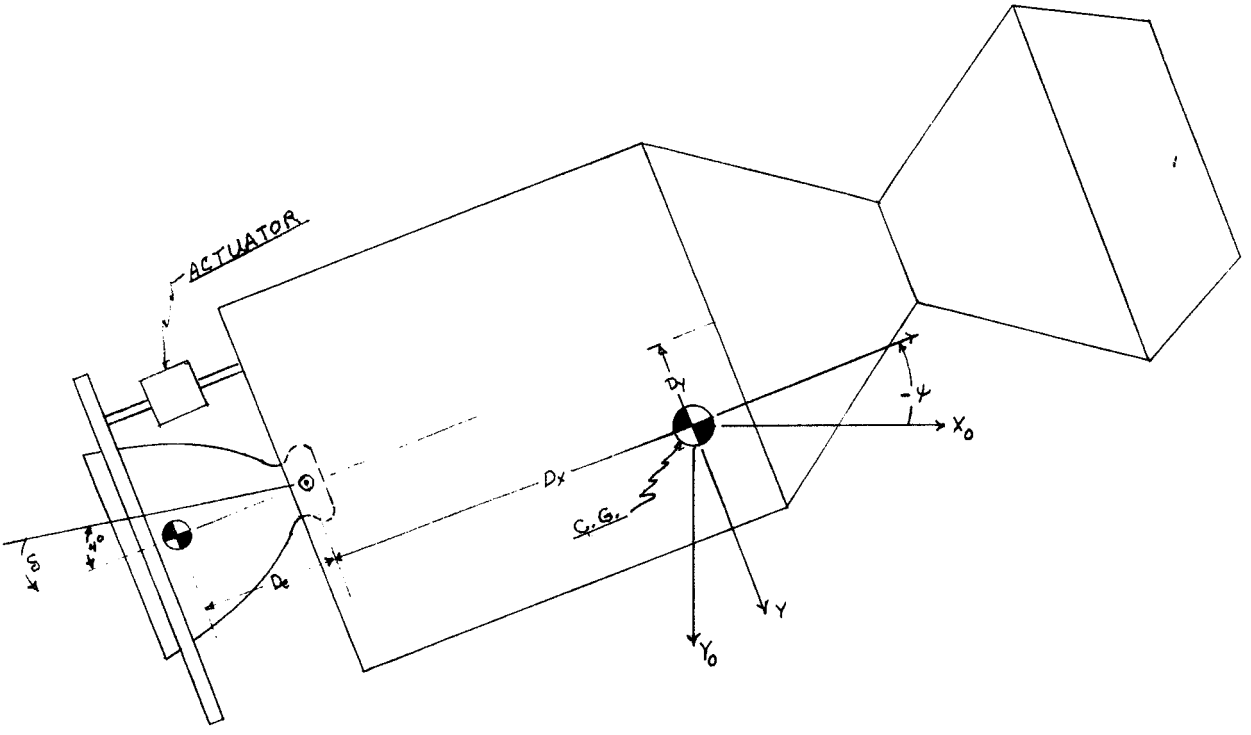

FIGURE 1

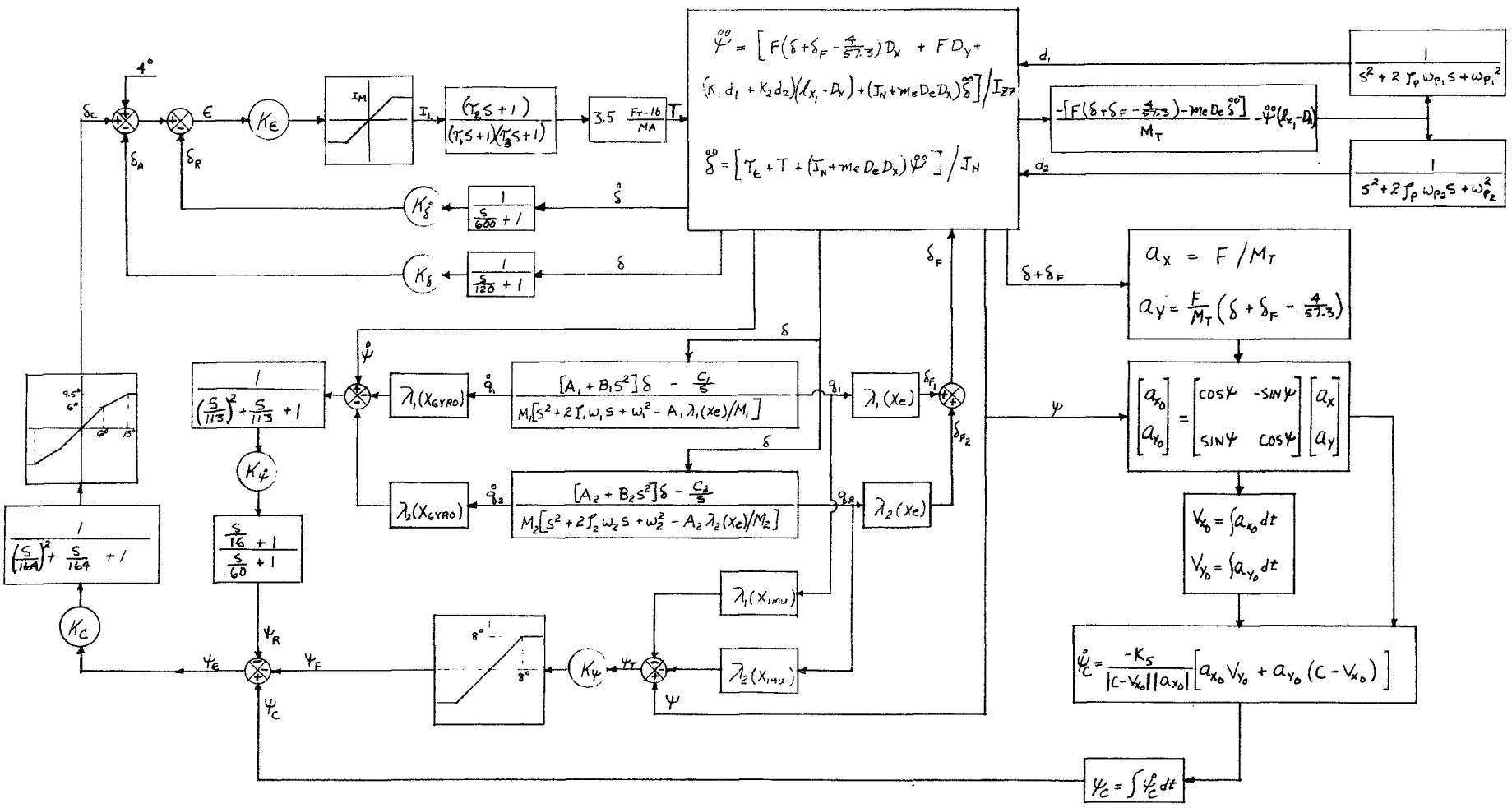
4°
δ_c
ϵ
K_ϵ
I_M
I_L
$\frac{(\tau_2 s+1)}{(\tau_1 s+1)(\frac{\tau_3}{3}s+1)}$
3.5 $\frac{Ft\text{-}lb}{MA}$
T
δ_A
δ_R
$K_{\dot\delta}$
$\frac{1}{\frac{s}{600}+1}$
$\dot\delta$
K_δ
$\frac{1}{\frac{s}{120}+1}$
δ
$\ddot\psi = \left[F(\delta+\delta_F-\frac{4}{57.3})D_X + FD_Y + (K_1 d_1 + K_2 d_2)(\ell_{X_1}-D_X) + (J_N + m_e D_e D_X)\ddot\delta\right]/I_{ZZ}$
$\ddot\delta = \left[\tau_\epsilon + T + (J_N + m_e D_e D_X)\ddot\psi\right]/J_N$
d_1
d_2
$\frac{1}{s^2+2\zeta_p\omega_{p_1}s+\omega_{p_1}^2}$
$\frac{1}{s^2+2\zeta_p\omega_{p_2}s+\omega_{p_2}^2}$
$\frac{-[F(\delta+\delta_F-\frac{4}{57.3})-m_e D_e\ddot\delta]}{M_T}$ $-\ddot\psi(\ell_{X_1}-D_X)$
δ_F
$\delta+\delta_F$
$a_X = F/M_T$
$a_Y = \frac{F}{M_T}(\delta+\delta_F-\frac{4}{57.3})$
$\dot\psi$
ψ
$\frac{1}{(\frac{s}{113})^2+\frac{s}{113}+1}$
K_ψ
$\lambda_1(X_{GYRO})$
$\dot q_1$
$\frac{[A_1+B_1s^2]\delta - \frac{C_1}{s}}{M_1[s^2+2\zeta_1\omega_1 s+\omega_1^2 - A_1\lambda_1(x_e)/M_1]}$
q_1
$\lambda_1(x_e)$
δ_{F_1}
$\lambda_2(X_{GYRO})$
$\dot q_2$
$\frac{[A_2+B_2s^2]\delta - \frac{C_2}{s}}{M_2[s^2+2\zeta_2\omega_2 s+\omega_2^2 - A_2\lambda_2(x_e)/M_2]}$
q_2
$\lambda_2(x_e)$
δ_{F_2}
$\begin{bmatrix}a_{X_0}\\a_{Y_0}\end{bmatrix} = \begin{bmatrix}\cos\psi & -\sin\psi\\ \sin\psi & \cos\psi\end{bmatrix}\begin{bmatrix}a_X\\a_Y\end{bmatrix}$
$V_{X_0} = \int a_{X_0}dt$
$V_{Y_0} = \int a_{Y_0}dt$
$\frac{1}{(\frac{s}{164})^2+\frac{s}{164}+1}$
$\frac{\frac{s}{16}+1}{\frac{s}{60}+1}$
$\lambda_1(X_{imu})$
$\lambda_2(X_{imu})$
K_C
ψ_R
ψ_E
ψ_F
ψ_C
K_ψ
ψ_T
ψ
$\dot\psi_C = \frac{-K_5}{|C-V_{X_0}||a_{X_0}|}\left[a_{X_0}V_{Y_0} + a_{Y_0}(C-V_{X_0})\right]$
$\psi_C = \int\dot\psi_C dt$

FIGURE 2